Supporting information

Carbon Supported Pt-Ni Oxygen Electrocatalysts as a Model to Follow Nickel Corrosion and Particle Detachment

Melina Zysler[a], Tal Klingbell[a], Charles D. Amos[b], Paulo J. Ferreira[b,c,d], and David Zitoun[a]

[a]*Department of Chemistry and Bar-Ilan Institute for Technology and Advanced Materials (BINA) Bar-Ilan University Ramat Gan 5290002, Israel.*

[b] *Department of Advanced Electron Microscopy, Imaging, and Spectroscopy, at the International Iberian Nanotechnology Laboratory (INL), Portugal.*

[c] *Materials Science and Engineering Program, The University of Texas at Austin, Austin, Texas 78712, USA*

[d] *Mechanical Engineering Department and IDMEC, Instituto Superior Técnico, University of Lisbon, Av. Rovisco Pais, 1049-001 Lisboa, Portugal.*

Experimental section

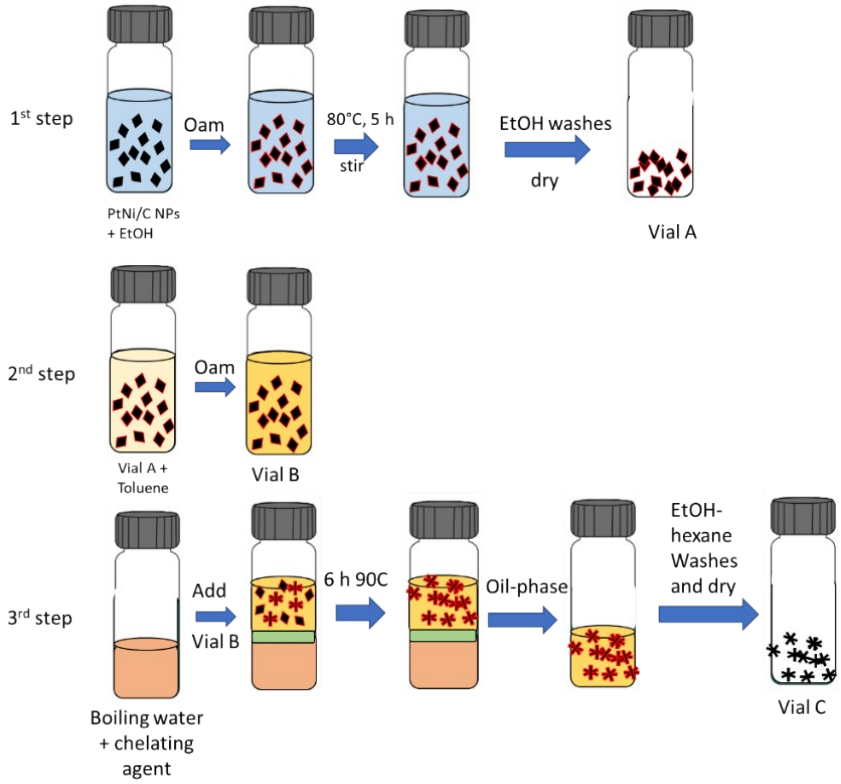

Figure S1. Scheme of two-phase corrosion process steps described in the experimental section.

Extra information

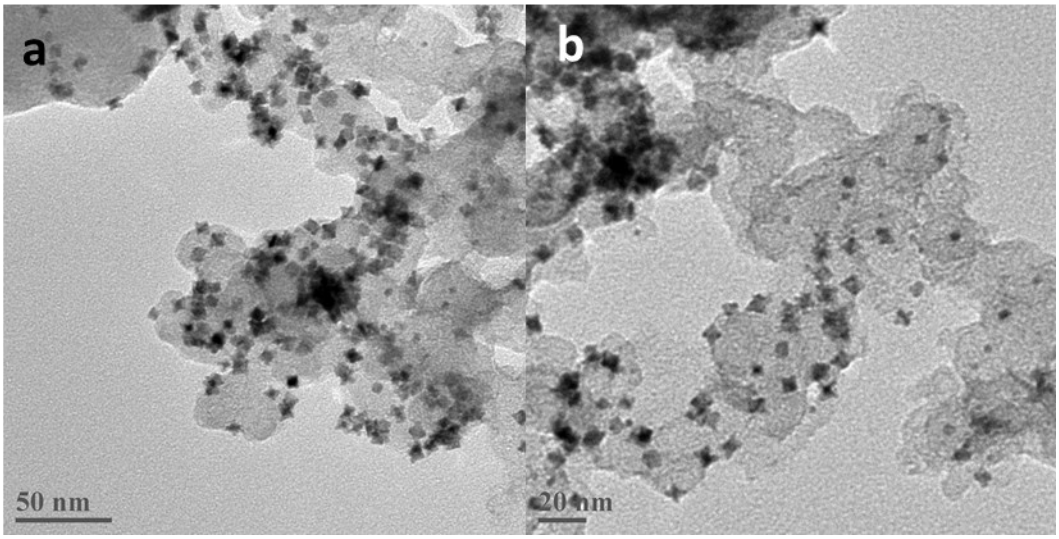

Figure S2. TEM bright-field images of sample 1-PtNi

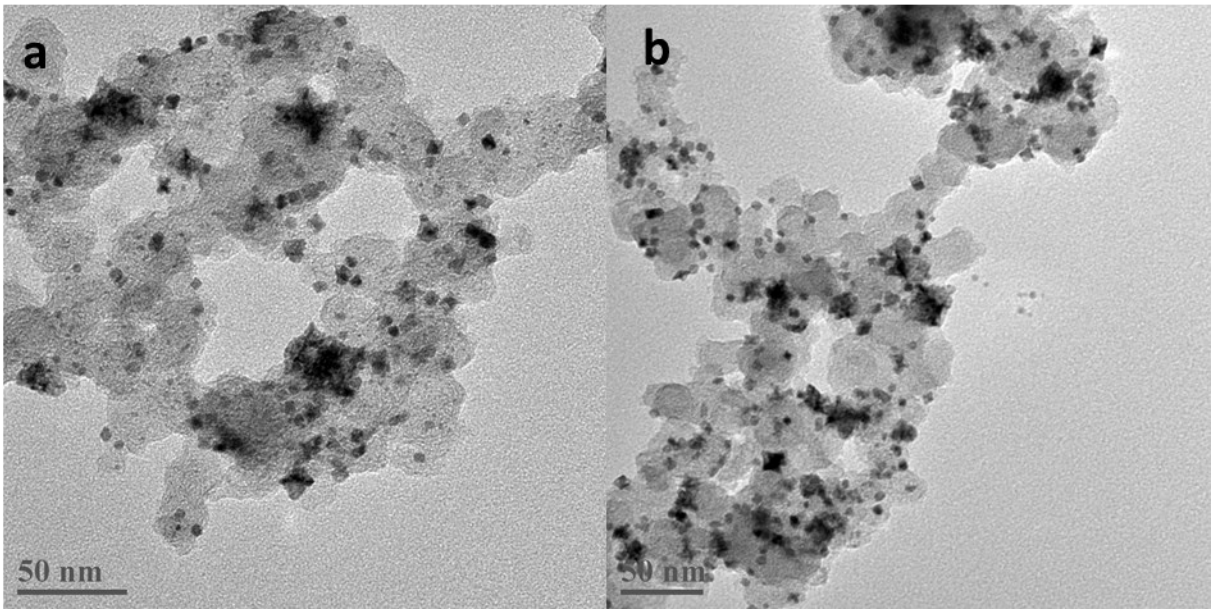

Figure S3. TEM bright-field images of sample 2-PtNi

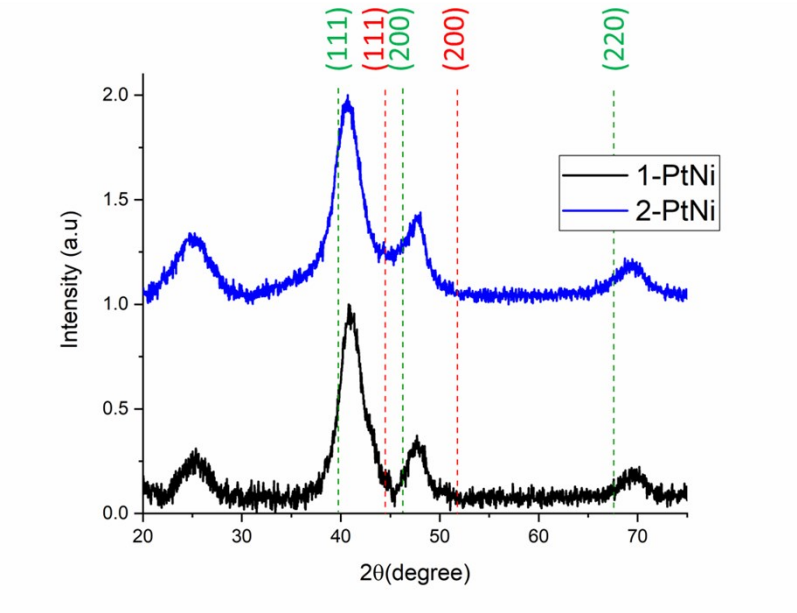

Figure S4. XRD patterns of Pt-Ni octahedral nanoparticles supported on carbon. 1-PtNi (black) and 2-PtNi (blue). Dashed lines correspond to the Pt (green) and Ni (red) standards. Pt (JCPDS no. 04-0802) and Ni (JCPDS no. 04-0850)

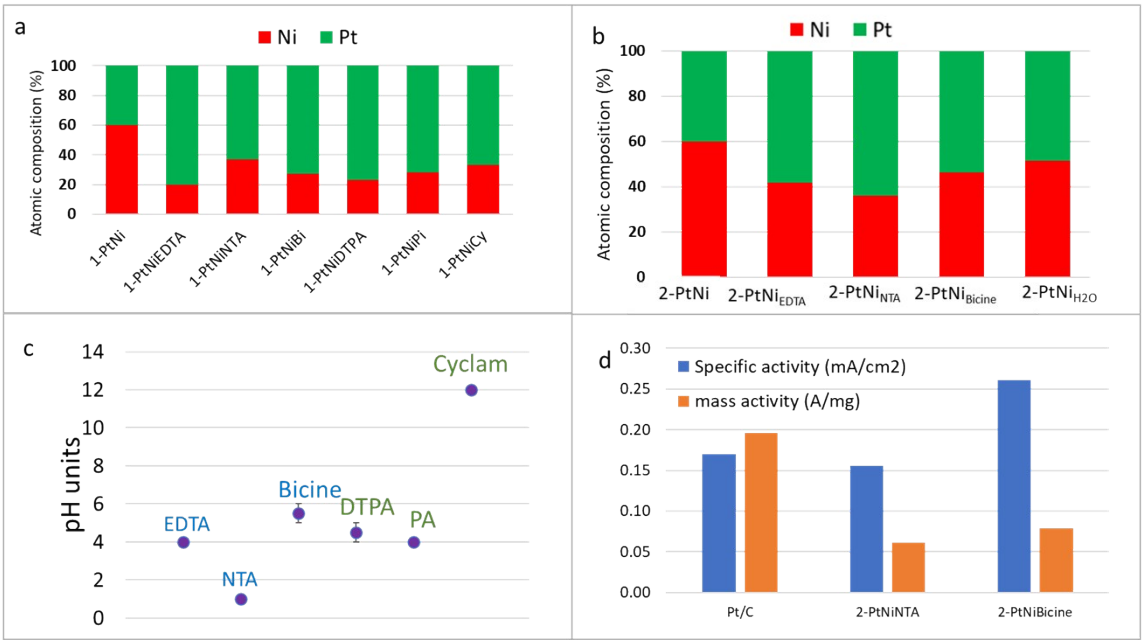

Figure S5. Properties of the Pt-Ni samples described in this work. Atomic metallic composition. (a) 1-PtNi and derivatives, (b) 2-PtNi and derivatives. (c) the pH of the aqueous phase of each of the batches and (d) electrochemical measurement comparison between Pt/C reference material,

2-PtNiNTA, and 2-PtNiBicine. Mass activity (A/mgPt, blue bars) and Specific activity (mA/cm2Pt, orange bars were calculated at 0.9 V (vs RHE). Measurements conditions are described in the Methods section.

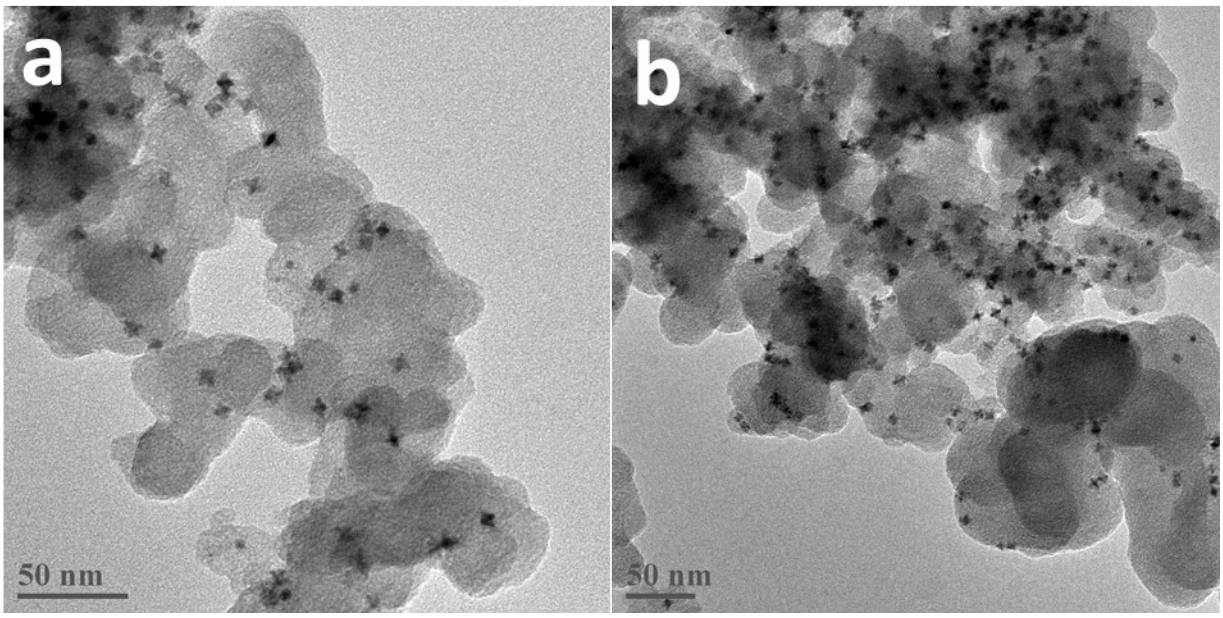

Figure S6. TEM bright-field images of sample 1-$PtNi_{EDTA}$

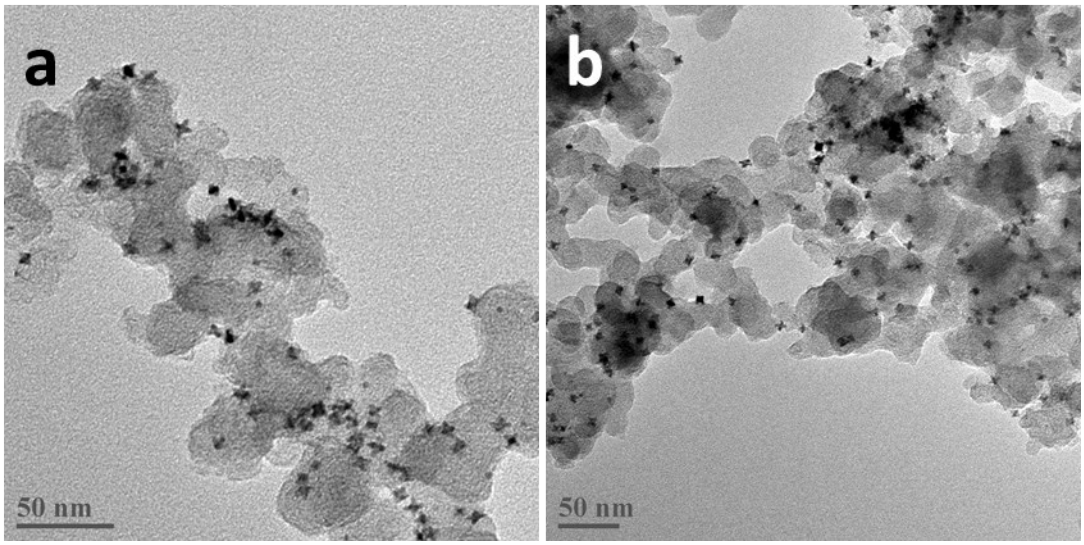

Figure S7. TEM bright-field images of sample 1-$PtNi_{NTA}$

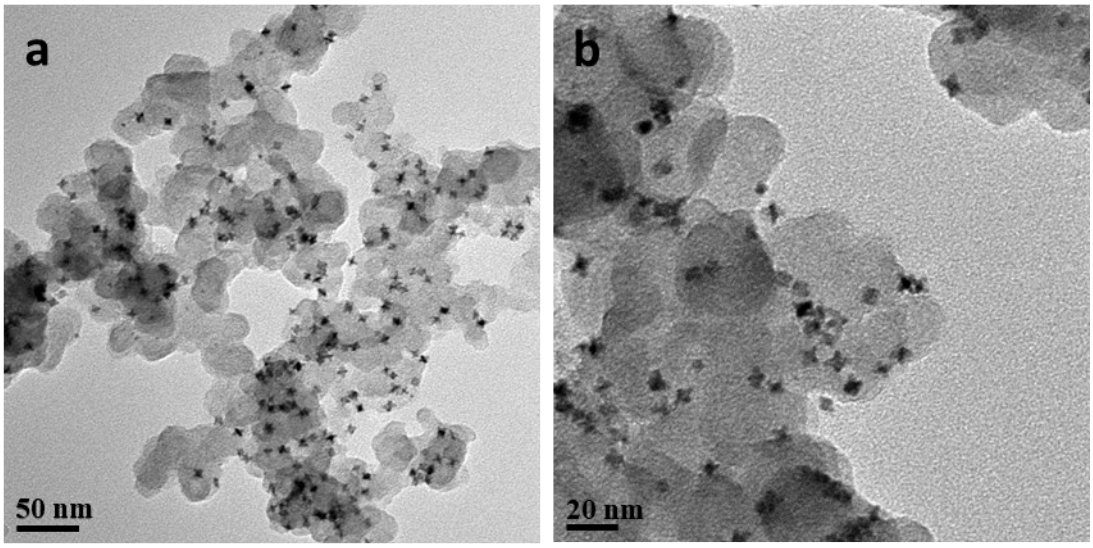

Figure S8. TEM bright-field images of sample 1-$PtNi_{Bicine}$

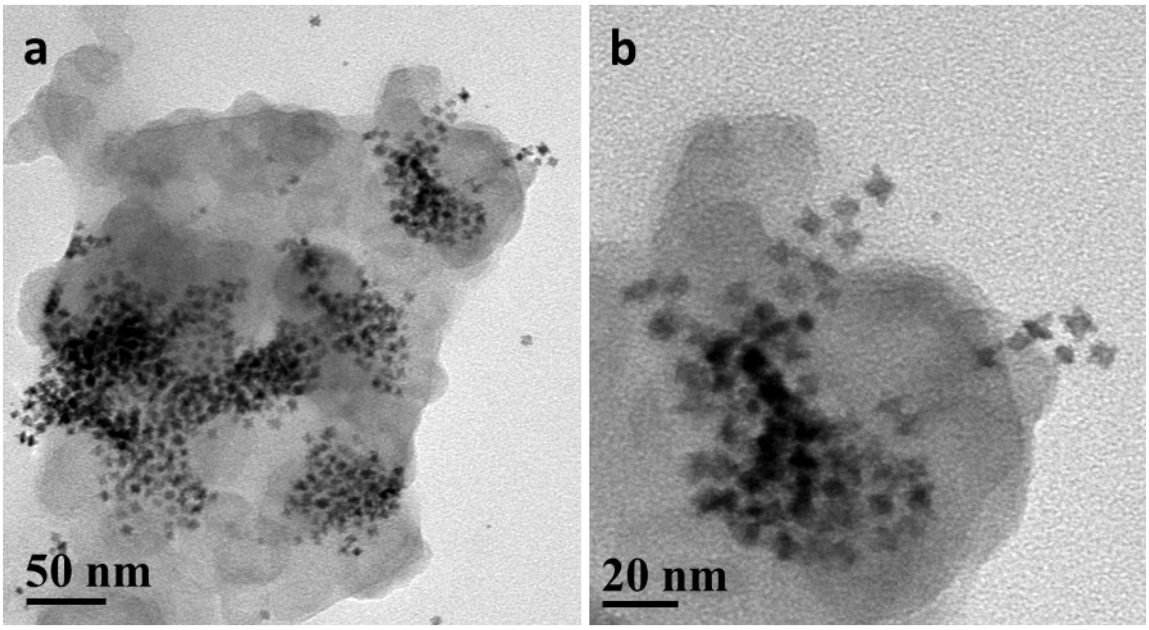

Figure S9. TEM bright-field images of sample 1-$PtNi_{DTPA}$

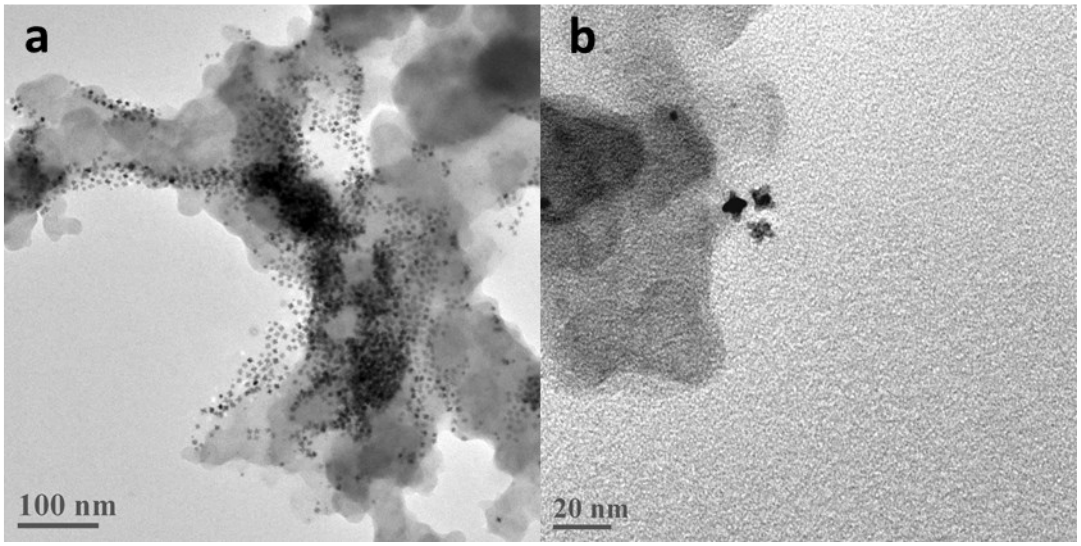

Figure S10. TEM bright-field images of sample 1-$PtNi_{PA}$

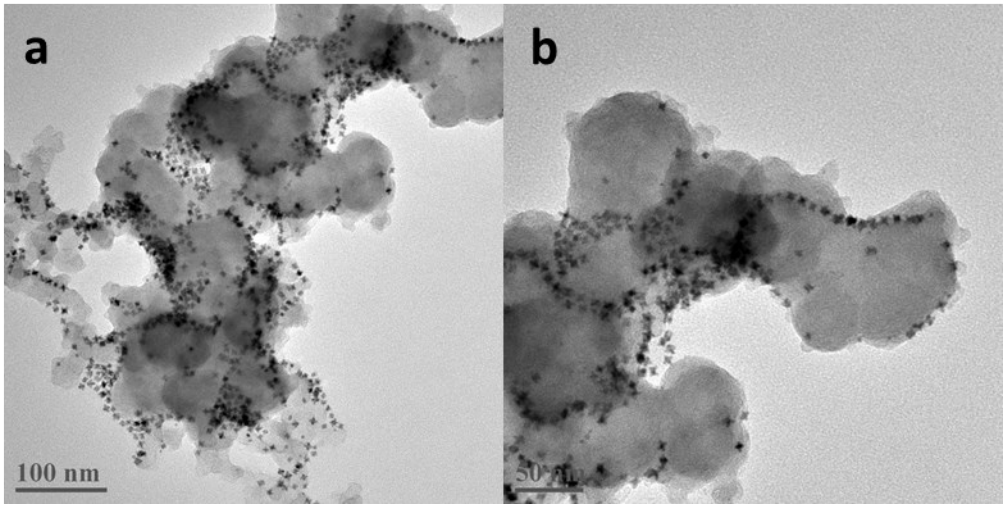

Figure S11. TEM bright-field images of sample 1-$PtNi_{Cyclam}$

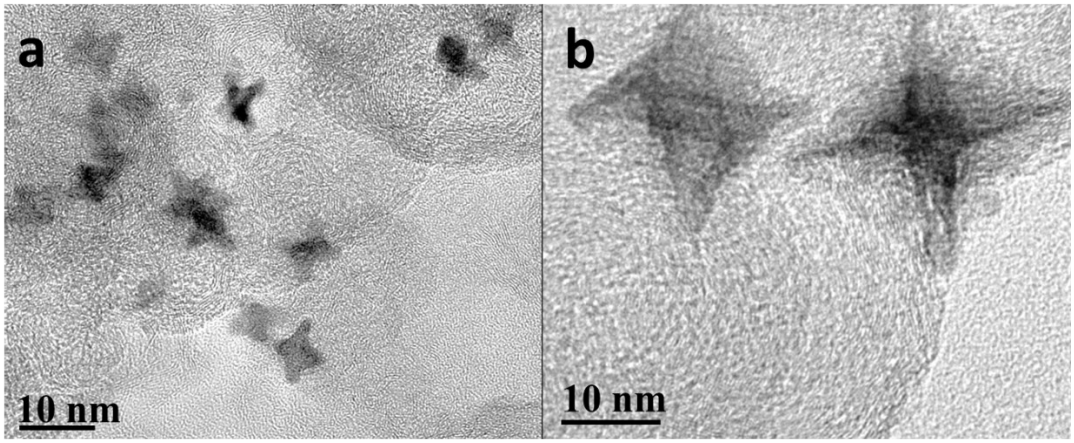

Figure S12. Phase contrast TEM images. (a) 1-$PtNi_{EDTA}$ and (b) 2-$PtNi_{NTA}$. Vulcan carbon support does not show modifications after the corrosion process

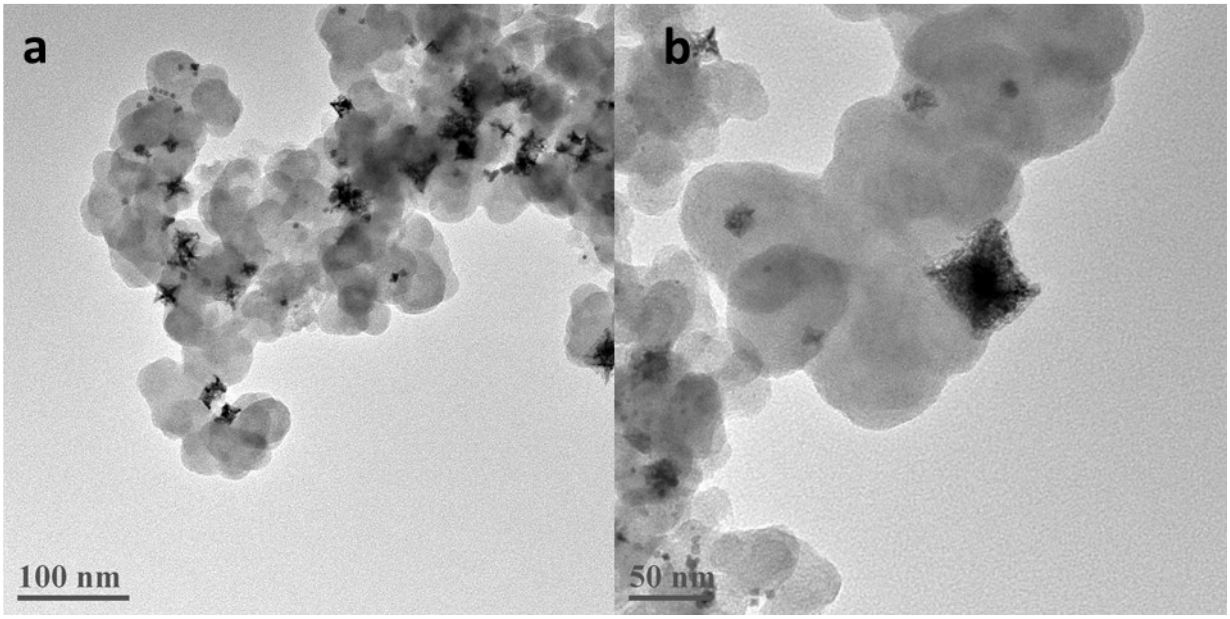

Figure S13. TEM bright-field images of sample 2-$PtNi_{EDTA}$

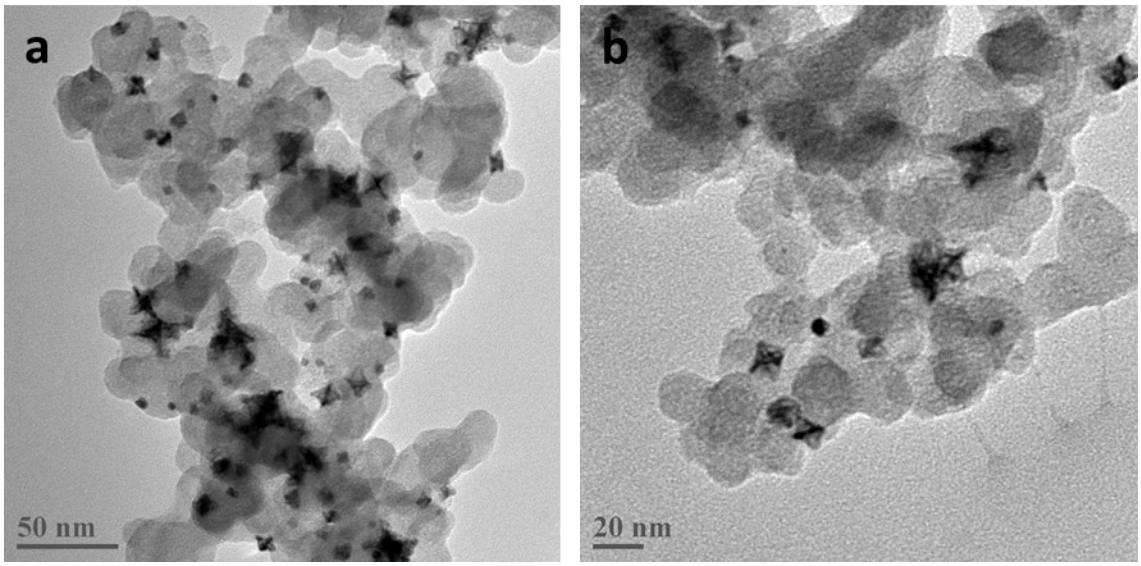

Figure S14. TEM bright-field images of sample 2-$PtNi_{NTA}$

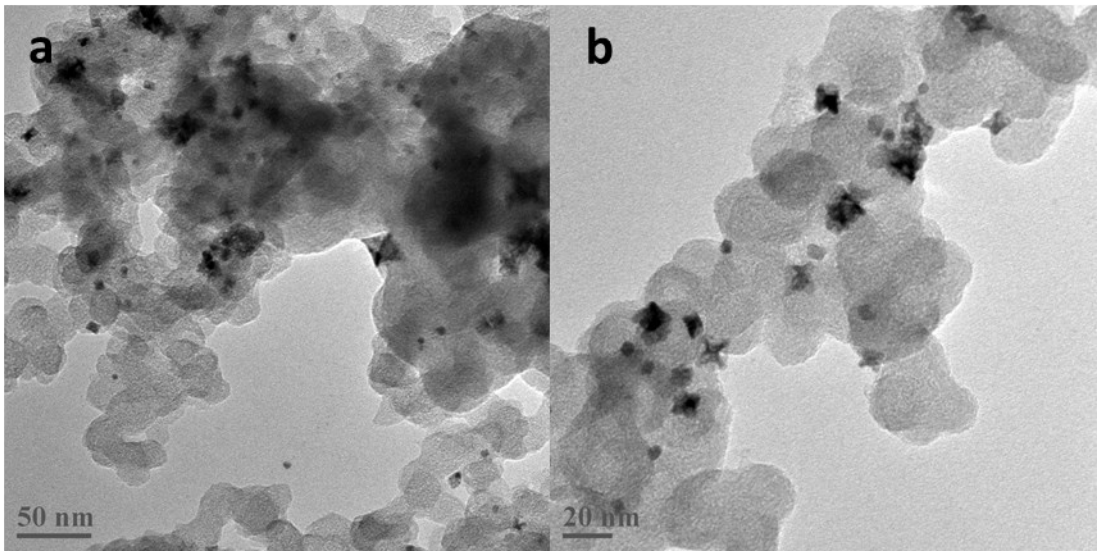

Figure S15. TEM bright-field images of sample 2-$PtNi_{Bicine}$

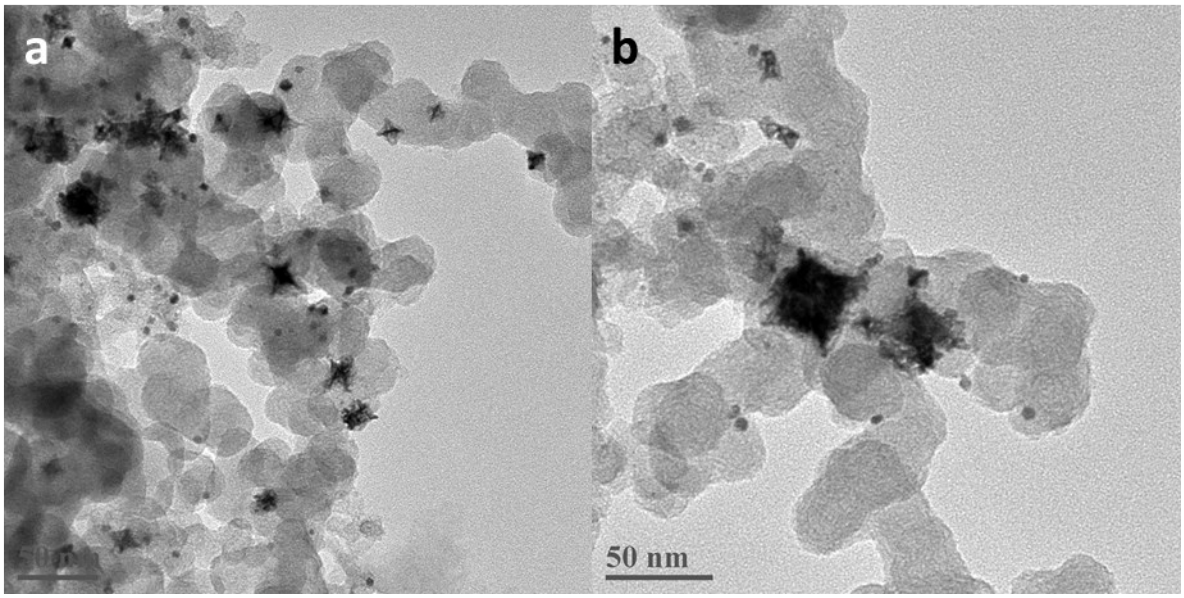

Figure S16. TEM bright-field images of sample 2-$PtNi_{H2O}$

Table S1. ICP-OES results for Pt-Ni octahedral NPs.

Sample	wt. $\%_{Pt}$	at. $\%_{Pt}$	at. $\%_{Ni}$	Formula
1-PtNi	12	40	60	Pt_2Ni_3
2-PtNi	16.6	40	60	Pt_2Ni_3
2-PtNi/OAm	13	50	50	PtNi
Ni-rich PtNi	3.5	15	85	$PtNi_6$

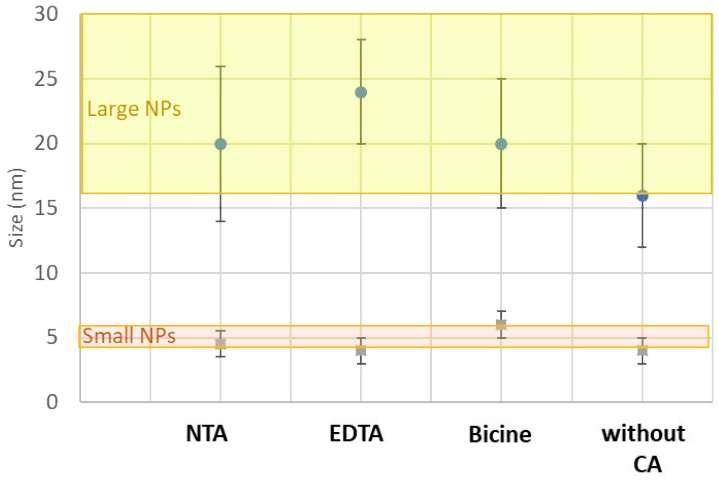

Figure S17. Size and standard deviation of 2-PtNi corroded octahedral NPs by different CAs and a control batch. 2-PtNi large particles' size is marked in the yellow region and 2-PtNi small particles' size is marked in the orange region.

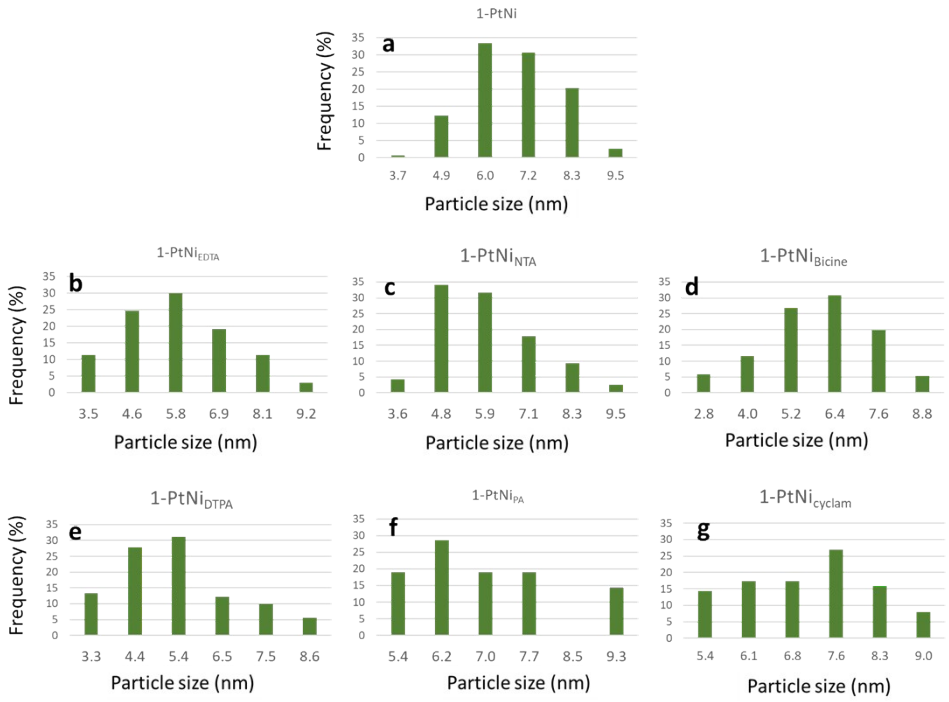

Figure S18. Nanoparticles size distribution for (a) 1-PtNi and all the derivate samples using different complexing agents. (b)1-PtNi$_{EDTA}$, (c) 1-PtNi$_{NTA}$, (d) 1-PtNi$_{Bicine}$, (e)1-PtNi$_{DPTA}$, (f) 1-PtNi$_{PA}$, and (g) 1-PtNi$_{cyclam}$. The particle size was obtained using ImageJ software and TEM bright-field images in which more than 200 particles were measured.

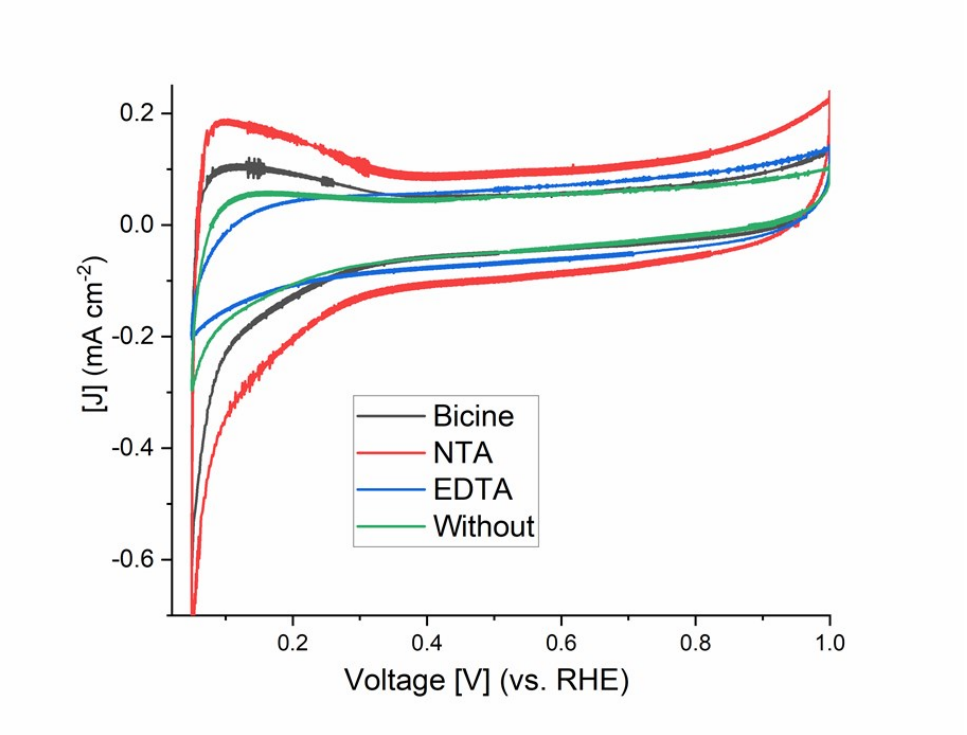

Figure S19. Cyclic voltammetry curves for 2-PtNi corroded samples. 2-$PtNi_{Bicine}$, 2-$PtNi_{NTA}$, 2-$PtNi_{EDTA,}$ and 2-$PtNi_{H2O}$.The measurements were performed at room temperature, 0.1 M $HClO_4$ argon saturated electrolyte. Scan rate 50 mV cm^{-2}, from 0.05 to 1 V (vs. RHE).

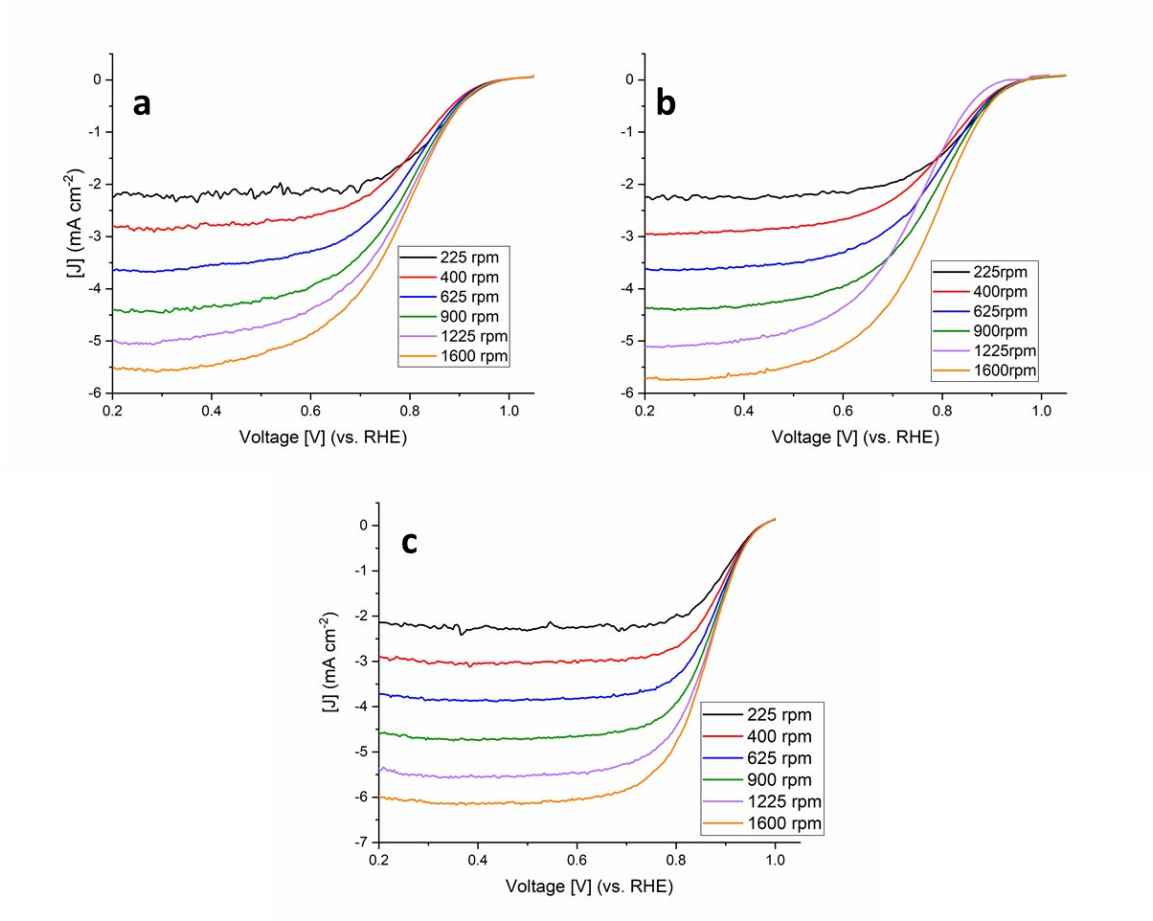

Figure S20. ORR polarization curves for 2-PtNi corroded samples and Pt/C reference. (a) 2-$PtNi_{Bicine}$, (b) 2-$PtNi_{NTA}$, and (c) Pt/C-JM reference material. The measurements were performed at room temperature, 0.1 M $HClO_4$ oxygen saturated electrolyte. Scan rate 20 mV cm^{-2}, from 0.2 to 1.05 V (vs. RHE), at different rotation speeds (only 1600 rpm curve was used for the activity calculations).

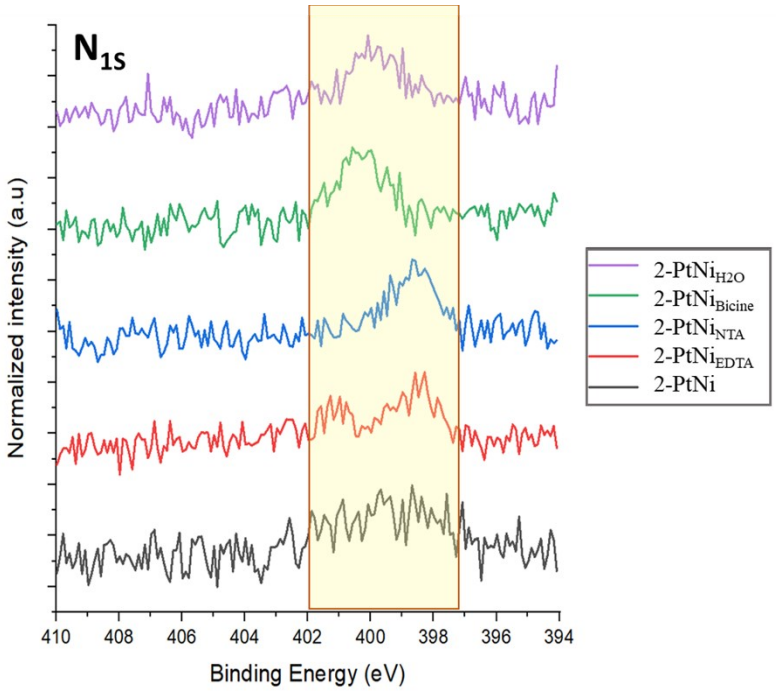

Figure S21. *High-resolution XPS characterization of 2-PtNi and 2-PtNi derivative samples in the N1s spectra region. 2-PtNi initial NPs (grey), 2-PtNi$_{EDTA}$ (red), 2-PtNi$_{NTA}$ (blue), 2-PtNi$_{Bicine}$ (green), and 2-PtNi$_{H2O}$ (purple).*

Characteristic peaks of nitrogen in the N1S region of the XPS spectrum were analyzed for 2-PtNi sample and the its derivatives generated by using complexing agents. The comparison of the relative intensities in this region (Figure SXX.) indicate presence of oleylamine observed in the 2-PtNi$_{H20}$ due to the peak situated around 400 eV, assigned to C-NH$_2$ compounds. In addition, 2-PtNi$_{EDTA}$ shows a second peak at higher energy binding that corresponds to the metal nitrides (that can be related to the complexing agent). The initial 2-PtNi do not reveal a peak but a noisy spectrum in which we believe that the nitrogen from the DMF remanent from the synthesis is contained.

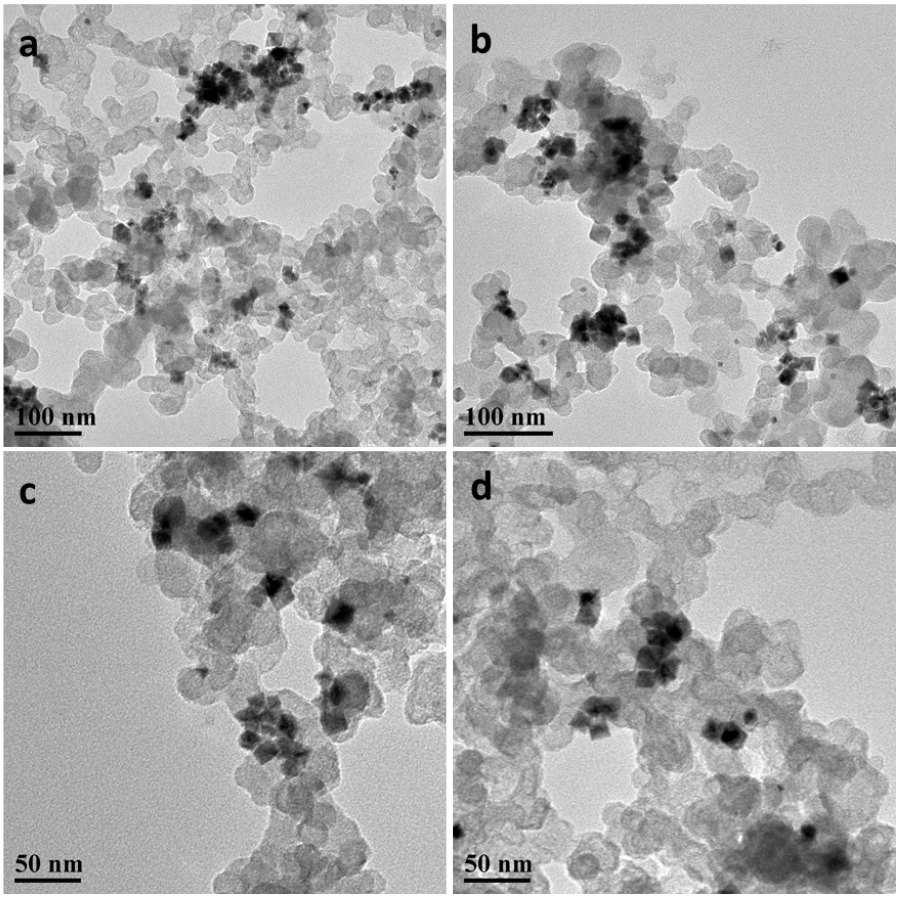

Figure S22. TEM bright-field images of sample Ni-rich PtNi ($PtNi_6$).

Remove a and d

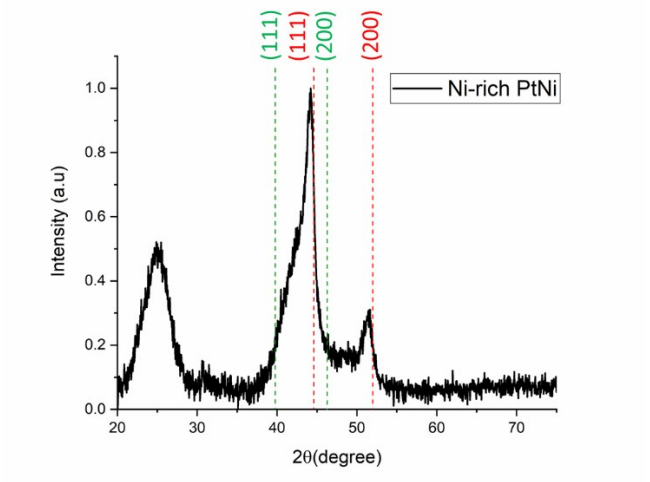

Figure S23. XRD pattern of Ni-rich Pt-Ni octahedral NPs supported on carbon. Dashed lines correspond to Pt (green) and Ni (red) standards. Pt (JCPDS no. 04-0802) and Ni (no. 04-0850)

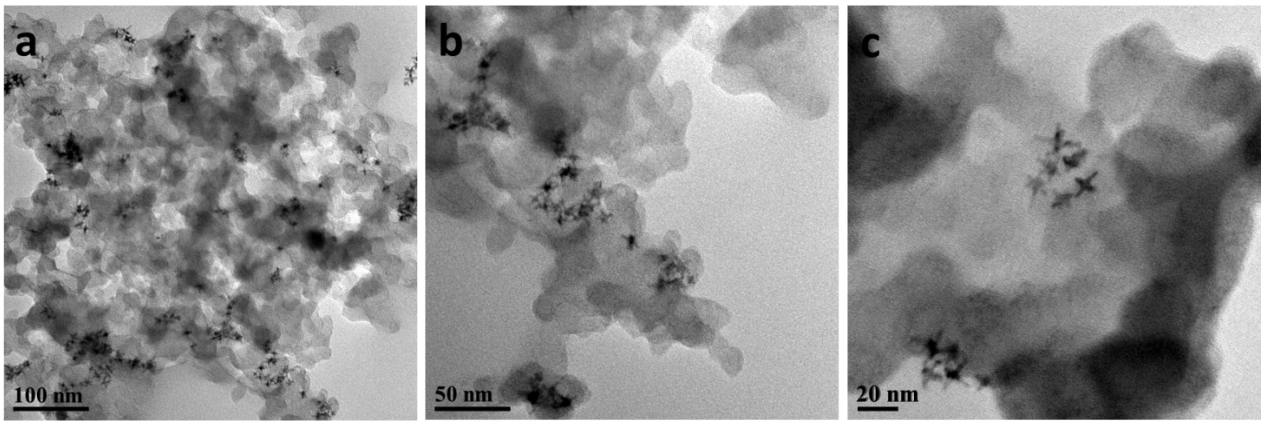

Figure S24. TEM bright-field images of sample Ni-rich PtNi ($PtNi_6$) after corrosion process using EDTA as a chelate agent.